Published in final edited form as:
Neuroscience. 2008 June 2; 153(4): 1048–1063. doi:10.1016/j.neuroscience.2008.02.060.

Stoned B Mediates Sorting of Integral Synaptic Vesicle Proteins

Ralf Mohrmann[*], **Heinrich J. Matthies**, **Elvin Woodruff III**, and **Kendal Broadie**
Department of Biological Sciences, Vanderbilt Kennedy Center for Research on Human Development, Vanderbilt Brain Institute, Vanderbilt University Nashville, Tennessee 37235-1634 USA

Abstract

A continuous supply of fusion-competent synaptic vesicles is essential for sustainable neurotransmission. *Drosophila* mutations of the dicistronic *stoned* locus disrupt normal vesicle cycling and cause functional deficits in synaptic transmission. Although both Stoned A and B proteins putatively participate in reconstituting synaptic vesicles, their precise function is still unclear. Here we investigate the effects of progressive depletion of Stoned B (STNB) on the release properties of neuromuscular synapses using a novel set of synthetic STNB hypomorphic alleles. Decreasing neuronal STNB expression to ≤35% of wildtype level causes a strong reduction in EJC amplitude at low stimulation frequencies and a marked slowing in synaptic depression during high-frequency stimulation, suggesting vesicle depletion is attenuated by decreased release probability. Recovery from synaptic depression after prolonged stimulation is also decelerated in mutants, indicating a delayed recovery of fusion-ready vesicles. These phenotypes appear not to be due to a diminished vesicle population, since the docked vesicle pool is ultrastructurally unaffected, and the total number of vesicles is only slightly reduced in these hypomorphs, unlike lethal *stoned* mutants. Therefore, we conclude that STNB not only functions as an essential component of the endocytic complex for vesicle reconstitution, as previously proposed, but also regulates the competence of recycled vesicles to undergo fusion. In support of such role of STNB, synaptic levels of the vesicular glutamate transporter (vGLUT) and synaptotagmin-1 are strongly reduced with diminishing STNB function, while other synaptic proteins are largely unaffected. We conclude that STNB organizes the endocytic sorting of a subset of integral synaptic vesicle proteins thereby regulating the fusion-competence of the recycled vesicle.

Keywords

synaptic vesicle cycle; endocytosis; stonin2; cargo sorting; synaptotagmin; vesicular glutamate transporter

Introduction

The maintenance of fast synaptic transmission requires the reconstitution of fusion-competent vesicles after phases of activity. Full vesicular fusion events inevitably deliver vesicular proteins to the plasma membrane, a process that occurs even at synapses that otherwise may

Corresponding author: Kendal S. Broadie, PhD, Professor, 6270 MRB III, 465 21st Avenue South, Nashville, TN 37232 USA, Tel: 615-936-3937 (office); -3935, -3936, and -6761 (lab); Fax: 615-936-0129, Email: E-mail: kendal.broadie@vanderbilt.edu.
[*]current address: Department of Membrane Biophysics, MPI for Biophysical Chemistry, D-37077 Göttingen, Germany

possess kiss-and-run style release. These “misplaced” vesicle proteins must be retrieved by consecutive sorting and uptake mechanisms. According to the classical model (Heuser and Reese, 1973), clathrin-mediated endocytosis (CME) represents the major mechanism for recovery of vesicle components after full fusion. Studies on receptor internalization during cellular housekeeping processes have identified a large set of proteins generally involved in CME (Schmid, 1997). However, relatively little is known about CME in the context of synaptic vesicle recycling.

Forward genetic screens in *Drosophila* have identified many proteins involved in synaptic vesicle cycling. The *stoned* gene locus was discovered in a screen for temperature-sensitive paralytic mutations 35 years ago (Grigliatti et al., 1973), and its dicistronic gene products were later named STNA and STNB (Andrews et al., 1996). Both Stoned proteins contain motifs common to CME accessory proteins, suggesting an involvement in endocytosis (Stimson et al., 1998). STNB shares partial homology with the μ2-subunit of AP-2. Viable and embryonic lethal *stoned* mutants suffer from compromised synaptic transmission at the neuromuscular junction (NMJ) synapse, and exhibit a delayed vesicular uptake of the styryl dye FM1–43, indicating a substantial slowing of vesicle recycling (Stimson et al., 1998; Fergestad et al., 1999; Stimson et al., 2001; Fergestad et al., 2001). Rescue experiments (Estes et al. 2003) attribute all major physiological defects to a specific loss of STNB in *stoned* mutants, with no known function attributed to STNA. However, despite this intriguing evidence that STNB function is essential for synaptic vesicle cycling, its specific role in endocytosis has not been sufficiently defined.

STNB clearly appears to regulate the trafficking of synaptotagmin-1, as the synaptic localization of the protein is disrupted in *stoned* mutants (Fergestad et al., 1999). Consistently, synaptotagmin-1 interacts directly with STNB *in vitro* (Phillips et al., 2000). Interestingly, Stonin2, the closest STNB vertebrate ortholog, is also proposed to act as a sorting factor for synaptotagmin-1, since Stonin2 overexpression stimulates the uptake of a synaptotagmin-GFP protein from the plasma membrane (Diril et al., 2006). Since synaptotagmin-1 is an essential modulator of Ca^{2+}-dependent neurosecretion (Tucker and Chapman, 2002), its mislocalization presumably contributes to the physiological impairments in *stoned* mutants. Synaptotagmin-1 is also suggested to be directly involved in the endocytic pathway of the synaptic vesicle cycle (Poskanzer et al., 2003; Nicholson-Tomishima and Ryan, 2004). Therefore, the mislocalization of synaptotagmin-1 in *stoned* mutants might directly participate in perturbing synaptic vesicle recycling.

In this study, we have engineered a set of novel *stnB* hypomorphic mutants to further investigate the function of STNB. We demonstrate that these *stnB* alleles have compromised basal synaptic transmission and altered synaptic depression during high frequency stimulation. However, these defects are not due to a diminished vesicle pool, but rather appear to arise from the compromised functional competence of synaptic vesicles in the mutants. In support of this idea, we demonstrate a selective depletion of the integral synaptic vesicle proteins synaptotagmin-1 and the vesicle glutamte transporter vGLUT in mutant presynaptic boutons, while other synaptic proteins are properly maintained. These results suggest that STNB is part of an endocytic sorting complex specific for a particular subset of integral membrane proteins during the reconstitution of synaptic vesicles.

Experimental procedures

Transgenic construct generation

A PCR fragment containing the STNB sequence was produced using the full-length cDNA clone RH38069 (BDGP collection; GenBank BT011172) as template. The PCR fragment was first inserted into the cloning vector pGEM-t (Promega) and subsequently cloned into the

pUASt vector (Brand and Perrimon, 1993) to yield the final construct (restriction sites: EcoRI and BglII). A truncated STNBΔMHD variant (amino acids 1–903) was generated using the alternative reverse primer 5′-GGA TCC TTA TGT CAA CGC TCG CTC TCG GAG AGC-3′. In addition, targeted mutations were introduced using Stratagene's QuickChange Kit employing the following primers: 5′-CC TCC GGA CAG GCC AAA GGC GAG CAT CAT CAC CG-3′ (Y1125G) and 5′-GCC ATT GTG TGG GCT TGT CCC CGT TTG CCC AAA G-3′ (R1135A). The double mutation Y1125G, R1135A was obtained by two successive rounds of mutagenesis. The chimeric STNB-AP50 construct was generated by fusion of three PCR fragments representing the N-terminal portion of STNB (amino acids 1–903), the homologous part of AP50 (amino acids 166–432; derived from cDNA clone SD05403), and the very C-terminal tail of STNB (amino acids 1219–1263). The strategy followed the widely used "Splicing by overlap extension"-method (Horton, 1995), and employed the overlapping primers: 5′-GAG CGA GCG TTG ACA TAC CGG CGC AAC GAG CTT TTC C -3′ and 5′-C ATC GGA CGC AGT GGC TTG GAG ACC ACG CAC GGC GAG -3′. 6xHis,myc-tagged STNB variants were produced by N-terminally attaching the sequence HHHHHHEQKLISEEDLNGGPR (c-myc epitope underlined).

Transgenic stock generation

Chimeric animals carrying insertions of UAS-constructs were generated by embryo injection using standard methods (Spradling and Rubin, 1982). Injected animals were mated to the *w1118* line, and progeny expressing the red eye-color marker w^+ due to successful p-element insertions were collected. All stocks were repeatedly back-crossed to *w1118*, while selecting for red-eyed progeny to retain the insertion. After at least three rounds of crossing, test-crosses were performed to map the chromosomal location of each p-element insertion. Homozygous and balanced stocks were generated using standard genetic techniques. The *w1118* stock was used as the genetic background control in all experiments.

Western Blot analysis

Heads of CO_2-anasthesized adults were manually removed with a razor blade and immediately frozen in liquid nitrogen. The tissue was then homogenized in sample buffer containing a protease inhibitor cocktail "2x complete" (Roche) as well as leupeptin (10μmol/ml) and pepstatin A (10μmol/ml). Protein extracts were subsequently electrophoresed using 4–20% SDS-PAGE gradient gels (Ready Gel, BIO-RAD) and transferred to a polyvinylidene difluoride membrane (Millipore). Stainings with antibodies directed against STNA/B (1:2000; Andrews et al., 1996; kind gift of Dr. L. Kelly), synaptotagmin (1:2000; kind gift by Dr. H. Bellen) and DAP160 (1:5000; Roos and Kelly, 1998) were performed in PBS (0.02 M phosphate buffer and 0.1 M NaCl, pH 7) containing Tween (Sigma) and 4% powdered milk. Immunopositive protein bands were visualized by using alkaline phosphatase-conjugated secondary antibodies with 5-bromo-4-chloro-3-indolyl phosphate and nitroblue tetrazolium as substrates (BIO-RAD). For analysis, blots were scanned, and band intensities were quantified using ImageJ software (NIH). Intensities for the different protein bands were normalized to the value of *w1118* controls on the same blot.

Electrophysiology

Two-electrode voltage-clamp (TEVC) recordings of the third instar larval NMJ were performed as previously described (Rohrbough et al., 1999). In brief, wandering third instar larvae were dissected in calcium-free standard saline (in mM: 128 NaCl, 2 KCl, 4 $MgCl_2$, 70 sucrose, 5 HEPES, pH 7.1). The dissected animal was transferred into fresh saline containing the appropriate extracellular calcium concentration and washed several times. Extracellular calcium concentration in recording bath saline was 1.8mM, unless otherwise noted. Recordings were done at 18°C in a temperature-controlled room. All recordings were performed in muscle

6 in anterior abdominal segment 3, using TEVC techniques (Axoclamp 2B amplifier; Axon Instruments). The holding potential was set to −60 mV in all recordings. Intracellular electrodes were filled with 3M KCl and had an average resistance of 10 MΩ. Excitatory junctional currents (EJCs) were evoked by application of brief stimuli (0.4–1ms; Grass Instruments S88 stimulator) to the cut motor nerve, using a glass suction electrode. Data acquisition and analysis was performed using pClamp software (version 8.0; Axon Instruments).

Electron microscopy

Mutant and wildtype control wandering third instar larvae were dissected, fixed, sectioned and visualized in parallel using standard transmission electron microscopy techniques, as reported previously (Rohrbough et al. 2007), with only minor changes. Briefly, animals were dissected in PBS and subsequently fixed with 2.0% glutaraldehyde in 0.05M PBS for 15 mins; replaced with fresh 2.0% glutaraldehyde for 1 hr. Preparations were washed three times in PBS, transferred to 1% O_sO_4 in dH_2O for 2 hrs, and then washed three times in dH_2O. Preparations were stained *en bloc* in 1% aqueous uranyl acetate for 1hr, washed three times in dH_2O, dehydrated in an ethanol series (30–100%), passed through propylene oxide, transferred to a 1:1 araldite: propylene oxide mixture, and embedded in araldite embedding media. Ultra-thin serial sections (50–60 nm) were made on a Leica UCT Ultracut microtome and transferred to 0.5% formvar-coated grids. Grids were examined and images collected on a Phillips CM10 TEM equipped with an AMT 2 mega pixel camera. NMJs were sectioned, and profiles for each synaptic bouton were quantified in sections containing only a single prominent electron-dense active zone (AZ) and T-bar structure. Synaptic vesicles in the “clustered” pool were defined as those within 250 nm of an AZ. Docked vesicles were defined as those <0.5 vesicle diameter (<20 nm) from the electron-dense plasma membrane at the AZ. Measurements and quantifications were made using ImageJ 1.32j free software from NIH. Each profile was scored for bouton/mitochondria area, and the number of docked, clustered vesicles and total vesicle density (corrected for mitochondria area). Mean quantified parameters were statistically compared using the Mann-Whitney test, and presentation images were processed in Adobe Photoshop CS.

Immunocytochemistry

Mature embryos (20–22 hrs after fertilization at 25°C) or wandering third instar larvae (96–106 hrs after hatching at 25°C) were dissected, and subsequently fixed in 4% paraformaldehyde in PBS (embryos: 20 mins; larvae: 45 mins). Bouin’s fixative was used for vGLUT immunostaining, as reported by Daniels et al. (2004). After permeabilization with 0.1% Triton X-100/PBS, preparations were incubated with primary antibodies at 4°C overnight. We used the following antibodies: anti-myc (1:500), anti-STNA/B (1:1000), anti-synaptotagmin1 (1:2000), anti-synaptobrevin (1:1000; Sweeney et al., 1995), anti-synapsin (1:200; Klagges et al., 1996; kind gift by Dr. E. Buchner), anti-vGLUT (1:500; kind gift by Dr. A. DiAntonio), anti-DAP160 (1:1000), and anti-horseradish peroxidase (HRP) (1:500; texas red conjugated; Jackson ImmunoResearch). Secondary anti-mouse and anti-rabbit antibodies (alexa488/633 conjugated) were obtained from Molecular Probes and were typically used at a dilution of 1:500 (2 hrs at room temperature). Images were collected on a Zeiss LSM 510 meta confocal microscope. All analysis was done using Zeiss LSM Image Examiner software. For quantification of immunointensities, projections of z-stacks were used of constant depths covering the axonal terminal ending. Regions of interest were drawn around presynaptic boutons by following the bouton geometry outlined with anti-HRP staining of presynaptic bouton membranes. Average pixel intensity within an area of interest was taken as a measure for synaptic expression of the protein within that individual presynaptic bouton. Since fluorescence data is typically not normally distributed, we calculated for each single NMJ the median of the intensities found in all presynaptic boutons. This value was then averaged and normalized to the mean value obtained for *w1118* controls in each type of staining.

Statistical analysis

All analysis of experimental data was done with InStat (Graphpad Software) or Clampfit (Axon Instruments). All data are given as mean ± S.E.M.

Results

Generation of a series of *stnB* hypomorphic mutant alleles

A set of novel *stnB* hypomorphic mutants was engineered to complement earlier studies on classical *stoned* mutants. To obtain animals with intermediate STNB expression levels, we employed the UAS-GAL4 system to drive expression of STNB in $stn^{13–120}$ mutant animals, which otherwise exhibit undetectable levels of endogenous STNB at neuromuscular synapses (Fergestad et al., 1999). Since positional effects have a strong impact on transgenic expression, we generated a collection of multiple lines of independent p{UAS-*stnB*} insertions, which could generate a variety of different STNB expression levels in combination with the neural-specific *elav*-GAL4 presynaptic driver. Hypomorphic animals were produced by crossing *elav*, $stn^{13–120}$/FM7i (kind gift of Dr. M. Ramaswami) virgins to males carrying p{UAS-*stnB*}, and unbalanced male larval progeny were collected. These animals are hemizygous with regard to the $stn^{13–120}$ allele, due to the X-chromosome localization of the *stoned* gene, but contain one copy of the *elav*-GAL4 driver as well as the specific p{UAS-*stnB*} transgene insertion.

Western Blot analyses of adult head extracts showed that three independent p{UAS-*stnB*} insertion lines produced an allelic series of STNB expression (Fig. 1A). The most severe hypomorph, which is referred to as *stn-vl* (very low expression), barely reaches the adult stage due to an inability to eclose from the pupal case. Surviving animals are highly uncoordinated and live only for a few days without special care. STNB expression level in the *stn-vl* animals was measured to be 34% (n=11) of the level found in wild-type (*w1118*; Fig. 1A). In contrast, the hypomorphic line *stn-l* (for low expression level) has significantly higher STNB levels (47% of *wt*; n=11), and survives at near normal rate. Most interestingly, these results indicate an expression threshold for STNB, between the levels found in *stn-vl* and *stn-l*, which is minimally required for normal survival to adulthood. A third hypomorphic line *stn-m* (for moderate expression level) exhibits the highest STNB expression (76% of *wt*; n=6) and appears undistinguishable from controls with respect to survival and coordinated movement.

To obtain a hypomorphic condition with even lower STNB expression, we took advantage of the pronounced temperature-sensitivity of the UAS-GAL4 system (Duffy, 2002). Raising *stn-vl* animals at 18°C decreased STNB expression to 20% of *wt* (n=6; Fig. 1A). Surviving adults were rare and extremely uncoordinated, with the majority of animals failing to eclose, presumably due to a lack of proper motor control. We also generated STNB over-expressing (OE) flies by crossing p{UAS-*stnB*} males to *elav-GAL4* virgins (Fig. 1A). Male progeny had 143% of the STNB expression of wildtype animals (n=6), but showed no obvious changes in viability or movement. Thus, we generated a 5-step, regularly graded series of STNB expression, compared to wild-type controls; 20%, 34%, 47%, 76% and 143%.

Like other *stoned* mutations, the $stn^{13–120}$ allele influences the expression of both STNA and STNB, since the coding sequences for both proteins form a fused, dicistronic transcription unit (Andrews et al., 1996; Wall et al., 2005). Interestingly, it was recently reported that transgenic expression of STNB rescues all *stoned* phenotypes in mutants that also critically affect STNA expression (Estes et al., 2003). Because of the special relationship of STNA/B we tested whether the transgenic expression of STNB affects the stability of STNA in $stn^{13–120}$ mutants, but did not observe an obvious correlation between the expression levels of both proteins (Fig. 1A). On western blots, STNA was detected as a group of bands with varying intensity patterns,

which might be due to partial degradation of the protein. The average amount of STNA in head fractions appeared nearly unaltered in all of the *stnB* hypomorphs compared to controls (*stn-vl* 18°C: 95%; *stn-vl* 22°C: 89%; *stn-l*: 96%; *stn-m*: 99%; n=6 each). However, in STNB overexpressing animals, we found a tendency towards increased STNA levels (132%; n=6; Fig. 1A).

We also analyzed the expression of the putative STNB binding partners DAP160 and synaptotagmin. DAP160 is recognized as a doublet band corresponding to two predicted isoforms. Average DAP160 levels were slightly reduced in the severe *stn-vl* hypomorph (72% at 18°C; 67% at 22°C; n=5 each), but were rather unchanged in milder hypomorphs and overexpressing animals (*stn-l*: 92%; *stn-m*: 89%; OE: 92% n=5 each; Fig. 1A). With progressive reductions in STNB expression, we also found a decrease in synaptotagmin expression level. Synaptotagmin was detected as a doublet band due to the occurrence of a hypersensitive trypsin cleavage site (Littleton et al. 1993; Fig. 1A), and showed considerable variability in hypomorphs. In *stn-vl* animals raised at 18°C, which exhibited the lowest STNB levels in our experiments, synaptotagmin expression was reduced to 70% (n=5) of control level. Synaptotagmin was slightly higher (80%) in *stn-vl* animals growing at 22°C (n=5). In *stn-l* and *stn-m* hypomorphs, the average synaptotagmin level was 89% and 107% of control level, respectively (n=5 each; Fig. 1A). Thus, there appears to be a dose-dependence of synaptotagmin maintenance on STNB level. In contrast, STNB overexpressing animals exhibited a normal synaptotagmin expression level (110%; n=5; Fig. 1A).

Defective basal synaptic transmission in severe STNB hypomorphic mutants

Lethal *stoned* mutations have a devastating effect on the integrity of the vesicle pools and neurotransmission strength (Fergestad et al., 1999). We therefore examined the role of STNB in sustained synaptic function in our new set of adult-viable hypomorphic mutants. Potentially, loss of STNB should cause altered synaptic vesicle pools or improper protein composition within synaptic vesicles, and consequently interfere with vesicle fusion. To check for changes in evoked synaptic transmission we recorded EJCs at the NMJs of wandering 3rd instar larvae (muscle 6, segment 3) using a basal stimulation frequency of 0.2Hz (1.8mM Ca^{2+}; Fig. 1B) to avoid pronounced synaptic depression (Fig. 2).

Control *w1118* and *elav-GAL4* animals exhibit average EJC amplitudes of 203.59.6nA (n=9) and 263.2±19.0nA (n=13), respectively (Fig. 1B). Note that there was a significant difference between the average amplitude of these two controls ($p<0.05$), emphasizing that differences in the genetic background produce a minor change in basal amplitude. In *stn-m* hypomorphs, average EJC amplitude was 236.2±7.0nA (n=13), indicating that the moderately reduced STNB expression level of STNB is sufficient for normal basal synaptic transmission (Fig. 1B). Average EJC amplitude in *stn-m* animals was not significantly different from that in the closely related *elav*-GAL4 control, but was slightly higher than in *w1118* animals ($p<0.05$). In *stn-l* hypomorphs, average EJC amplitude was 234.7±8.5nA (n=11), which was also indistinguishable from *stn-m* and *elav* animals, demonstrating that even a >50% reduction of STNB expression still allows for normal basal synaptic transmission (Fig. 1B). In contrast, further decreased STNB expression in the severe *stn-vl* hypomorphs produced a 40% reduction in average EJC amplitude (141.3±10.7nA, n=8, $p<0.001$ compared to *elav* and *w1118*). Thus, it appears that a certain STNB expression level is required for basic synaptic function. This threshold lies roughly at ~40% of *wt* expression, right between the expression levels of *stn-vl* (34%) and *stn-l* animals (47%). Raising *stn-vl* animals at lower temperature (18°C), to further reduce STNB expression, significantly decreased the average amplitude of EJCs to 101.4 ±11.0nA (n=9, $p<0.05$ compared to *stn-vl;* $p<0.0001$ in comparison with *elav* and *w1118*; Fig. 1B). We also recorded EJCs in the viable *stoned* allele *stnC*. The *stnC* mutants are not simple hypomorphs, as an early stop in the STNB coding sequence yields a truncated STNB isoform,

which is also accompanied by some full-length, read-through product (Kelly and Phillips, 2005). These mutants exhibited an average EJC amplitude of 76.5±6.8nA (n=8; Fig. 1B), which is a slightly more pronounced defect than in *stn-vl* hypomorphs. Kelly and Phillips (2005) reported that full-length STNB was expressed at extremely low levels in *stnC* animals (slightly over 10% of *wt* in P3 fractions of head extracts). Assuming that truncated STNB is not biologically active, the *stnC* phenotype therefore further expands on the tight correlation between functional impairment and expression below a threshold STNB level. STNB overexpression did not measurably alter synaptic function, as basal EJC amplitude in over-expressing animals (OE) was not significantly different from either genetic control (235.3 ±18.0nA, n=8; Fig. 1B).

In summary, we find that a severe reduction of STNB expression significantly depresses basal synaptic transmission. Below a certain threshold, the efficacy of basal synaptic transmission shows a close dose-dependence on STNB level.

Synaptic depression is altered in severe STNB hypomorphic mutants

To characterize dynamic transmission properties and overall performance, neuromuscular synapses were subjected to prolonged high-frequency stimulation followed by a period of recovery. Similar paradigms have recently been used to unveil functional deficits in endophilin and synaptojanin mutants (Verstreken et al., 2002, 2003; Dickman et al., 2005). The applied stimulation paradigm consisted of a 1 minute baseline interval with stimulation at 0.1Hz, a 10 minute interval with high-frequency stimulation (HFS) at 10Hz to strongly challenge synapses, and a subsequent recovery interval with 0.1Hz stimulation (Fig. 2).

In *w1118* controls, the synaptic response pattern during HFS exhibited strong depression, consisting of an initial rapid decrease in EJC amplitude, followed by a slow progressive amplitude reduction (Fig. 2B). Recovery after the end of the HFS train showed a biphasic profile reminiscent of the depression kinetics, with a rapid initial amplitude recovery succeeded by a delayed phase of slow recovery. In controls, recovery reached almost the full initial amplitude by the end of a 14 minute recovery interval. Normalized EJC amplitude plots were nearly identical for *w1118* (n=7) and *elav-GAL4* (n=7) control animals. The profile for *stn-m* hypomorphs (n=7) was also not significantly different for these controls (Fig. 2B). Even in low expressing *stn-l* hypomorphs (47% of normal STNB), the normalized response profile did not show any significant alterations compared to control animals (n=9; Fig. 2C). However, in the very low expressing *stn-vl* animals (n=10), which also exhibited a reduction in basal EJC amplitude, two major deviations from the normal response pattern were evident (Fig. 2D): First, as the most prominent change, the overall recovery from synaptic depression was dramatically slowed in *stn-vl* animals, with only a 60% average recovery after 14 minutes. This result is readily explained by an inefficient vesicle recovery delaying the refilling of the depleted vesicle pool. Second, the initial rapid depression during HFS was clearly less pronounced in *stn-vl* hypomorphs than in controls (Fig. 2G), although the relative depression at the end of the 10Hz stimulus train was comparable to that in controls.

For *stn-vl* hypomorphs raised at 18°C, which expressed STNB at the lowest levels, this slowing of initial depression during HFS was significantly more pronounced (Fig. 2E, G). Surprisingly, recovery from depression was less affected at 18°C than at 22°C, reaching ~75% of basal control amplitude (Fig. 2E). This might indicate that depression and recovery kinetics reciprocally depend on each other. Consistent with this possibility, the rate of synaptic depression in the *stnC* mutant animals was slower than for *stn-vl* animals, while recovery was considerably faster and was more complete than in *stn-vl* hypomorphs (Fig. 2F, G). It is noteworthy that the effect of HFS plasticity was so dramatically altered in in *stnC* mutants, that in several cases (5 out of 13 experiments) depression was briefly preceded by an initial period of facilitation.

To better compare the changes in depression kinetics, EJC amplitude plots during the initial 3 minutes of HFS were fit with a monoexponential function. Though a single time constant does not fully describe depression kinetics, it still provides a useful measure of the timecourse of initial depression. For cases in which facilitation initially occurred, the fit interval was adjusted to the period following the peak amplitude to avoid invalid fits of the data. The averaged time constant was 17.6±1.8s in *w1118* animals. In *stn-vl* hypomorphs raised at 22°C or 18°C the time constants were significantly ($p<0.01$ and $p<0.05$) increased to 32.9±3.8s and 42.5±7.2s, respectively. The average time constant in *stnC* mutants was also significantly ($p<0.0001$) prolonged to 46.4±3.0s.

To further our analysis of synaptic depression in STNB hypomorphic mutants, we systematically applied short test trains of 40 stimuli at different frequencies, determined the relative residual amplitude by averaging the last five responses in each train, and normalized this amplitude to the control amplitude evoked at 0.2Hz. EJCs were elicited at 1Hz, 5Hz, 10Hz, and 20Hz (Fig. 3A). Synaptic depression in *w1118* (n=7) and *elav* control animals (n=10) increased progressively with frequency (*w1118*: 74.5±0.6% at 1Hz, 56.9±2.0% at 5Hz, 52.7 ±1.6% at 10Hz, 37.1±2.6% at 20Hz; *elav*: 75.6±2.4% at 1Hz, 56.9±3.4% at 5Hz, 53.3±3.4% at 10Hz, 44.3±4.0% at 20Hz). Similar to basal synaptic transmission, the *stn-m* and *stn-l* hypomorphs with moderate to strong STNB reduction appeared completely normal under these stimulation paradigms (*stn-m*: 75.4±1.8% at 1Hz, 61.3±1.4% at 5Hz, 55.4±1.6% at 10Hz, 43.6 ±2.9 at 20Hz; *stn-l*: 76.2±0.7% at 1Hz, 58.8±2.0% at 5Hz, 53.4±2.1% at 10Hz, 44.4±2.4% at 20Hz). Only the very low-expressing *stn-vl* hypomorphs (22°C) exhibited a significantly ($p<0.05$) altered depression profile for frequencies ≥5Hz (Fig. 3A). Frequency-dependent depression was again clearly less pronounced in *stn-vl* hypomorphs than in controls (22°C: 76.8±1.5% at 1Hz, 68.5±2.0% at 5Hz, 64.4±2.6% at 10Hz, 55.7±3.3% at 20Hz, n=8). On average depression was also slightly milder in *stn-vl* raised at 18°C than in animals raised at room-temperature (*stn-vl* 18°C: 79.8±2.4% at 1Hz, 74.3±4.2% at 5Hz, 78.6±6.8% at 10Hz, 71.4±8.1% at 20Hz, n=9; for ≥5Hz: $p<0.01$ compared to *w1118*), though this alteration was not statistically significant. *stnC* mutants also exhibited significantly ($p<0.01$) less synaptic depression for frequencies ≥5Hz (80.9±2.0% at 1Hz, 80.7±5.7% at 5Hz, 82.3±6.7% at 10Hz, 76.3±8.3% at 20Hz, n=7; Fig. 3A); for frequencies ≥10Hz depression was even significantly ($p<0.05$) milder than in *stn-vl* hypomorphs (22°C).

If depression at the NMJ synapse is primarily caused by vesicle pool depletion, it can be reasoned that both the reduction in basal EJC amplitude and the accompanying reduced depression are indicators of a decreased release probability. Like most forms of short-term plasticity, paired-pulse facilitation/depression (PPF/D) is considered to be very sensitive to changes in the initial release probability, but should not reflect any use-dependent deficits in the re-supply of vesicles by endocytosis. Hence, PPF/D was tested in *stn-vl* (22°C) and *stnC* animals, compared to *w1118* control animals and moderate *stn-m* hypomorphs, which were indistinguishable from controls in previous experiments (Fig. 3B). Paired stimuli were applied with interstimulus intervals (ISI) of 25, 50, and 100ms using an extracellular calcium concentration of 1.8mM. As expected, *w1118* and *stn-m* exhibited very similar amplitude ratios (A_2/A_1) for all ISIs (*w1118*: 77.7±1.7% for 25ms, 87.6±0.9% for 50ms, 87.9±1.0% for 100ms, n=8; *stn-m*: 75.5±2.2% for 25ms, 84.5±0.8% for 50ms, 86.7±0.6% for 100ms, n=9; Fig. 3B). In severe *stn-vl* hypomorphs, the amplitude ratio A_2/A_1 was not significantly different from *w1118* and *stn-m* for a short 25ms ISI (80.0±3.2%, n=10), but PPD was slightly, but significantly reduced at ISIs of 50 and 100ms (93.0±1.6% for 50ms, 92.5±1.5% for 100ms, $p<0.05$). Most interestingly, *stnC* mutants showed a switch from depression to facilitation at each ISI (111.6±3.6% for 25ms, 106.9±4.5% for 50ms, 105.6±4.2% for 100ms, n=7, $p<0.001$; Fig. 3B). Thus, short-term synaptic plasticity in severe STNB hypomorphs and *stnC* mutants was consistently affected under various stimulation paradigms. However, at low calcium concentrations (0.2 mM), PPF was similar in all genotypes (*w1118*: 186.2±14.8% for 25ms,

171.5±11.0% for 50ms, 146.4±11.0% for 100ms, n=8; *stn-m*: 172.8±8.4% for 25ms, 158.8 ±7.8% for 50ms, 140.6±4.3% for 100ms, n=8; *stn-vl*: 173.0±13.6% for 25ms, 156.3±10.2% for 50ms, 129.6±8.3% for 100ms, n=8; *stnC*: 187.2±5.3% for 25ms, 160.4±14.4% for 50ms, 149.7±8.4% for 100ms, n=5; Fig. 3B). This is presumably because the facilitating effect of increased residual calcium was more pronounced than the adverse effect on release probability.

In summary, synapses in severe *stnB* hypomorphic mutants suffer from defective basal synaptic transmission as well as from altered synaptic depression. Both changes can be most consistently explained by a decreased release probability of synaptic vesicles.

Severe STNB hypomorphic mutants exhibit only minor ultrastructural changes

Our previous work on the lethal *stoned* alleles showed that a critical loss of STNB disrupts normal vesicle cycling, and results in a vesicle depletion as well as an accumulation of membrane recycling intermediates (Fergestad et al., 1999). To correctly interpret the *stnB* hypomorphic physiological phenotypes, i.e. defective basal synaptic transmission and decreased depression, it was crucial to investigate the integrity of the presynaptic vesicle pools at the ultrastructural level. For this purpose, electron microscope sections through the NMJ synapses on longitudinal muscles of the anterior abdominal segments (A2–A4) were obtained from *w1118* control, and *stn-m* and *stn-vl* mutant animals (Fig. 4).

The bouton area (μm^2), total vesicle number, number of clustered vesicles per profile, the number of docked vesicles per profile, and the overall density of synaptic vesicles were quantified (Fig. 4 and data not shown). As expected, profiles from *w1118* (n=55) and *stn-m* hypomorphs (n=39) did not show any significant differences in the number of clustered vesicles (*w1118*: 15.7±0.6; *stn-m*: 17.6±1.0*)* and docked vesicles (*w1118*: 1.71±0.12; *stn-m*: 1.79±0.14) at presynaptic active zones, or overall vesicle density throughout the bouton (*w1118*: 80.3±5.6 vesicle/μm^2; *stn-m*: 85.1±5.4 vesicle/μm^2; Fig. 4A, B). In *stn-vl* hypomorphs, the focus of interest due to their physiological phenotype, the number of clustered vesicles (16.4±0.8) and docked vesicles (1.88±0.13) was not significantly different from controls (n=43; Fig. 4A, B). However, overall vesicle density was slightly reduced to 62.6±5.5vesicle/μm^2, a 22% decrease compared to *w1118* ($p<0.05$). Kuromi and Kidokoro (1998) demonstrated that fast cycling synaptic vesicles generally form a pool located near the bouton periphery at the *Drosophila* NMJ, while reserve pool vesicle are typically found at the center of the synaptic boutons. This fast cycling pool is presumably vastly overlapping with the readily releasable pool (Kuromi and Kidokoro, 2003), which has been electrophysiologically defined in this preparation (Delgado et al., 2000). For *stn-vl* hypomorphs, our ultrastructural data reconfirms the integrity of this vesicle pool, as vesicle density near the active zone is normal (Fig. 4). Interestingly, depletion of the readily releasable pool should be the predominant process shaping the initial phase of depression during synaptic activity, and thus the observed change in depression is presumably due to changed functional properties of these vesicles.

Please note that profiles in *stn-vl* had a tendency to cover smaller areas (*w1118*: 4.22 ±0.36μm^2; *stn-vl*: 3.40±0.37μm^2; p=0.12; Fig. 4) indicating that bouton geometry might be changed in a subset of boutons. We also observed an overall increase in the amount of extra membrane in the form of cisterna among the synaptic vesicles in *stn-vl* mutants (data not shown), which may contribute to the smaller bouton diameter. These phenotypical features indicate a subtle endocytic defect, which does not affect the vesicle pool, but may be responsible for the delayed recovery of NMJs after prolonged activity.

Synaptic vesicle proteins are differentially affected by loss of STNB

The above functional analyses suggest that synaptic vesicles display a progressively reduced release probability with progressive lower STNB activity. We therefore tested directly for

evidence of vesicle protein sorting/trafficking defects in *stoned* mutants by performing quantitative immunohistochemistry of the integral vesicle proteins synaptobrevin, synaptotagmin, and the vesicular glutamate transporter vGLUT (Fig. 5). We also examined the expression pattern of synapsin, which is envisioned to dynamically associate with and dissociate from synaptic vesicle membranes depending on its phosphorylation state (Hosaka et al., 1999), and thus presumably does not depend on endocytic sorting mechanisms. Assays were done on third instar NMJs of *w1118* control, and *stn-m*, and *stn-vl* hypomorphic alleles. Presynaptic protein expression levels were quantified by measuring the fluorescence intensity throughout all of the presynaptic boutons at a single identified NMJ, visualized for this purpose with a texas red conjugated anti-horseradish peroxidase (HRP) antibody that recognizes the presynaptic plasma membrane (Fig. 5). Pixel fluorescence intensity measurements obtained for synaptic boutons typically form skewed distributions. We therefore relied on the median rather than the mean intensity for comparing fluorescence intensities.

Fluorescence intensities for synaptobrevin (SYB), synaptotagmin (SYT), and synapsin (SYN) were very similar in *w1118* controls and *stn-m* hypomorphs, a condition, which did not exhibit a physiological phenotype (Fig. 5). Normalized bouton intensity in *stn-m* animals was 96.0 ±6.2% for SYB (n=15 NMJs, 1088 boutons; *w1118*: 100.0±5.5%, n=15 NMJs, 776 boutons), 98.0±5.6% for SYT (n=17 NMJs, 996 boutons; *w1118*: 100±3.7%, n=14 NMJs, 791 boutons) and 112.8±6.9% for SYN (n=16 NMJs, 972 boutons; *w1118*: 100.0±4.7%, n=16 NMJs, 778 boutons) relative to *w1118* animals (Fig. 5B). Surprisingly, however, *stn-m* exhibited a significant reduction in vGLUT levels (71.3±2.6%, n=12 NMJs, 773 boutons) compared to *w1118* animals (100.0±3.3%, n=19 NMJs, 948 boutons, $p<0.00001$), which indicates that the synaptic localization of vGLUT is very sensitive to a loss of STNB (Fig. 5A, B).

Interestingly, the severe *stn-vl* hypomorphs showed a significant reduction in the presynaptic expression level of every vesicle-associated protein tested, although the effect clearly fell into two well-defined categories. There was a severe reduction in the levels of the two integral vesicle proteins, SYT and vGLUT. SYT fluorescence intensity was highly significantly reduced in the *stn-vl* hypomorphic condition (49.9±3.5%, n=17 NMJs, total: 971 boutons, $p<0.00001$), suggesting a specific defect in the localization of SYT to synaptic vesicles (Fig. 5). The decrease in SYT synaptic expression in *stn-vl* was significantly more pronounced than either SYN or SYB ($p<0.001$ and $p<0.01$, respectively). Likewise, vGLUT level was also highly significantly reduced to a stronger degree in severe *stn-vl* hypomorphs (46.9±1.8%; n=18 NMJs; 1299 boutons; $p<0.00001$; Fig. 5). In contrast, SYB and SYN were clearly less dependent on STNB. SYB level was reduced by ~30% (68.6±5.4%, n=17 NMJs, 1405 boutons, $p<0.001$), and also SYN was decreased by a similar level (71.3±4.3%, n=14 NMJs, 635 boutons, $p<0.0001$; Fig. 5). This ~30% decrease in SYN and SYB synaptic levels parallels the similar decrease in overall vesicle density shown at the ultrastructural level (Fig. 4).

A reduction in synaptic vesicle proteins might be accompanied by a mislocalization of vesicle proteins to inappropriate sites. Previous studies have suggested that synaptotagmin is mislocalized in animals carrying lethal *stoned* mutations (Fergestad et al., 1999). Therefore, we further examined mutant synapses at higher magnification for qualitative changes in SYB, SYT, vGLUT, and SYN (Fig. 6). HRP antibody staining was used to visualize the morphology of axonal branches and synaptic boutons. The morphology of boutons in moderate *stn-m* hypomorphs was comparable to that found in *w1118* control animals. However, we did observe characteristic morphological alterations in *stn-vl* hypomorphs. Synaptic boutons, especially in terminal regions of axonal branches, frequently were not normally shaped. Typically, the oval bouton shape was lost and aggregates of smaller boutons seemed to form instead (Fig. 6). These morphological alterations appeared very similar to satellite boutons that were reported to also occur in several other endocytic mutants (Dickman et al., 2006). In many cases, the spacing of normally shaped boutons was decreased, and boutons did not follow the size distribution

patterns of Is and Ib boutons. In contrast, the majority of synaptic boutons in the central regions of the axonal branches had normal morphological features. Average bouton size was quantitatively compared between mutants and *w1118* control by determining maximum cross-sectional areas of individual boutons in confocal stack projections. We found no difference between the average bouton areas in *stn-m* and *w1118* animals (*stn-m*: 3.37±0.48μm^2, n=15; *w1118*: 3.64±0.25μm^2, n=15). In contrast, in *stn-vl* animals average bouton area was highly significantly reduced by ~30% compared to *w1118* and *stn-m* animals (2.42±0.11μm^2; n=17; $p<0.0001$), consistent with the smaller synaptic bouton profiles measured in the ultrastructural analysis. It should be noted that we did not make a distinction between Is and Ib synaptic boutons, as this classification could not be clearly applied to the abnormally shaped boutons in *stn-vl* mutants.

Vesicle-associated proteins are typically found accumulated in the bouton cortex near the plasma membrane, and mostly excluded from the central region of boutons (Fig. 6). The *stn-vl* hypomorphs often exhibited protein distributions that did not well correspond to this typical 'doughnut' staining pattern. However, because we observed no clear, systematic pattern of 'mislocalization' of the vGLUT, SYB and SYN proteins, it may be that these abnormalities are a secondary effect of perturbed morphology. The exception was SYT, for which we found a systematic shift in immunoreactivity closer to and overlapping with the plasma membrane (Fig. 6B). Similar observations have been previously reported by Stimson et al. (2001) for *stnC* mutants. These results support the conclusion that SYT is mistrafficked in the absence of STNB activity, with a severity correlating with the degree of STNB removal.

In summary, our immunocytochemical analyses suggest that the synaptic expression of several vesicle proteins is differentially regulated by STNB. In severe *stn-vl* hypomorphs, SYB and SYN expression was reduced by ~30%, confirming the mild reduction in vesicle density observed in EM profiles. Strikingly, however, SYT and vGLUT staining levels were more severely reduced, which suggests a differential dependence of synaptic protein localization on STNB.

Unilateral localization/stabilization of SYT by STNB

Direct binding between STNB and SYT has been shown based on biochemical experiments *in vitro* (Philips et al., 2000). Since our results indicated a strong dependence of synaptotagmin upon STNB, we further investigated whether a STNB-SYT interaction mutually stabilizes both binding partners at synaptic sites, or whether STNB unilaterally stabilizes synaptotagmin at terminals. To answer these questions we performed immunohistochemical stainings against STNB in embryonic lethal syt^{AD4} null mutants (DiAntonio et al., 1993; Broadie et al., 1994). NMJs in mature syt^{AD4} mutant embryos (20–22hrs after fertilization) showed a moderate reduction in synaptically localized STNB (Fig. 7A). In contrast, however, synaptic expression of synaptotagmin was very much more severely reduced in $stn^{13–120}$ mutants, indicating that the STNB-SYT interaction is more critically important for SYT stabilization at synaptic sites, rather than a mutually dependent requirement.

Recent work by Kelly and Phillips (2005) further proposed a direct interaction between STNB and DAP160, the *Drosophila* homologue of intersectin (Roos and Kelly, 1998). A loss of DAP160 has recently been shown to affect the localization of a wide range of endocytic proteins, in addition to causing defects in bouton morphology (Koh et al., 2004; Marie et al., 2004). Since DAP160 is therefore considered an organizer of endocytic proteins, we tested whether the absence of DAP160 alters the synaptic expression of STNB, or vice versa (Fig. 7). For this purpose, we stained embryonic NMJ terminals for STNB in $DAP160^{\Delta 1}$ mutants (kind gift of Dr. H. Bellen), and also analyzed DAP160 expression in embryonic lethal $stn^{13–120}$ mutants. $DAP160^{\Delta 1}$ mutants are considered null for DAP160, and are lethal at 3rd instar (Koh et al., 2004). In both mutants, the synaptic expression of the genetically unaffected

corresponding protein was only moderately reduced (Fig. 7C, D). Therefore, it appears unlikely that a hierarchical dependence exists between STNB and DAP160 with respect to the mechanism of their synaptic localization.

In summary, testing for mutual stabilizing/localization activity between STNB and its putative binding partners reconfirmed again the exceptional dependence of presynaptic SYT expression on STNB, while STNB localization was not affected by a loss of its binding partners. Also DAP160 localization seems to be vastly independent of STNB activity.

Mutations in the μ2 homology domain cause defects in STNB localization

The mislocalization of SYT in *stnB* hypomorphic mutants may partly explain their physiological phenotypes. To directly address the importance of the interaction between STNB and SYT, we generated mutant variants of STNB predicted to alter or abolish its affinity for SYT (Fig. 8A). To disrupt the μ2 homology domain (MHD), the defined site of SYT interaction (Phillips et al., 2000), we constructed a STNB variant (STNBΔMHD) lacking the MHD as well as the short consecutive C-terminal tail. This C-terminally truncated protein variant should be unable to interact with SYT or any other MHD binding partner. To specifically weaken the STNB-SYT interaction, we constructed an additional variant mutated within the putative synaptotagmin-binding site within the MHD. Haucke et al. (2000) previously reported that the SYT-AP50 interaction is nearly eliminated by the mutation of two amino acids, which are conserved in STNB. We therefore introduced similar mutations at these positions (Y1125G and R1135A). The resulting STNB variant was named STNB Y1125G, R1135A (Fig. 8A). The STNB MHD, although similar to that of AP50, possesses some short unmatched stretches and is slightly larger than its counterpart, which might indicate altered functional properties. To investigate the interchangeability of both domains, we constructed a *STNB-AP50 chimera*, in which we replaced the STNB MHD with the corresponding sequence of AP50. Surrounding sequences, including the short c-terminal tail, were left intact (Fig. 8A). Each STNB variant was N-terminally epitope-tagged with a His-tag (6xHis) and a Myc-tag to enable detection. All constructs were subcloned into pUASt vector and were then introduced into the genome by germline transformation. A tagged wildtype STNB construct was generated to serve as control.

Rescue experiments demonstrated that pan-neuronal expression (*elav*-GAL4) of the tagged wildtype STNB could restore viability in lethal $stn^{13–120}$ animals. In contrast, however, none of the mutant STNB variants could rescue lethal *stoned* mutants. While these results demonstrate the importance of an intact MHD, it was especially surprising that the *stnB-AP50 chimera* did not support even a partial rescue. Hence, the homologue sequences in STNB and AP50 apparently do not encode functionally equivalent domains. We further characterized the mutant STNB variants by neuronally expressing the different STNB forms in a wildtype background, and studied their localization by immunostaining for the *myc* epitope (Fig. 8). In the ventral nerve cord (VNC) of third instar larvae, tagged wildtype STNB was concentrated within the synapse rich-region of the neuropil, as expected for STNB as a synapse-associated protein (Fig. 8B). Tagged STNB was only marginally detectable in the somata of VNC neurons. Moreover, tagged wildtype STNB was similarly heavily concentrated in presynaptic boutons of NMJs on bodywall muscles (Fig. 8D). In sharp contrast, 6xHis, *myc*-STNBΔMHD could not be detected at all in the synaptic neuropil, and was also absent from NMJ synapses (Fig. 8C, D). Large amounts of the truncated STNB protein were found in somata of VNC neurons, where they formed a punctate pattern. 6xHis, *myc*-STNB Y1125G, R1135A was also undetectable in the central synaptic neuropil and at NMJ synapses (Fig. 8C, D). Similar to truncated STNB, this version was mainly expressed in the cell bodies of VNC neurons, but in contrast to the truncated ΔMHD product, its localization was homogenously distributed within the soma and sometimes was also found in proximal neurites. Possibly, this STNB variant is

able to passively diffuse into dendrites, but is presumably not actively transported to synaptic sites. Finally, the distribution of the *STNB-AP50 chimera* was strikingly similar to the localization of the truncated ΔMHD STNB variant; it was never observed in the CNS synaptic neuropil and also appeared to be completely absent at NMJ synaptic boutons (Fig. 8). Within somata, the chimeric protein also showed typical punctate accumulations that appeared indistinguishable from the pattern found for the truncated protein. Therefore, the chimeric protein behaved in every way as if it completely lacked a functional MHD.

In summary, manipulations targeting the MHD have a strong impact on STNB protein localization and/or transport. Truncated STNB without MHD and the *STNB-AP50 chimera* are not synaptically localized, and remain in the soma of neurons. If the SYT interaction site is mutated, STNB also was not detectable at any synaptic sites, but was rather trapped, homogenously distributed within the soma.

Discussion

The *Drosophila stoned* locus was identified 35 years ago based on severe behavioral impairments (Grigliatti et al., 1973). It is one of the few dicistronic loci characterized in *Drosophila*, encoding Stoned A and B proteins; however, the Stoned A protein appears totally dispensable for known functions (Estes et al., 2003). In contrast, the crucial importance of the Stoned B protein for synaptic transmission has been well established (Stimson et al., 1998; Fergestad et al., 1999). Nevertheless, the exact mechanistic function of STNB remains enigmatic. Here we have generated and characterized a graded set of STNB hypomorphic animals to provide evidence that STNB has a dose-dependent limiting function regulating neurotransmission strength as a potent sorting factor governing a specific set of integral vesicular proteins during synaptic vesicle reconstitution. The key findings supporting this interpretation of STNB function are (I) the occurrence of diminished and altered release in a progressive series of STNB hypomorphic alleles, in the absence of significant ultrastructural defects of the vesicle pools, thereby indicating a changed fusion competence of synaptic vesicles, and (II) the differential loss of integral synaptic vesicle proteins dependent on the level of STNB activity.

In previous studies, severely compromised basal synaptic transmission has been reported as a prominent feature of the physiological phenotype of various classical *stoned* mutants (Stimson et al., 1998; Fergestad et al, 1999). Simplistically, defective synaptic release might be entirely a secondary effect of a primary impairment in vesicle pool maintenance, due to disrupted vesicle endocytosis. However, recent studies of *endophilin* and *synaptojanin* endocytic mutants suggest that only a surprisingly small number of synaptic vesicles is actually required to support normal synaptic function at basal stimulation frequencies: In both *endophilin* and *synaptojanin* mutants, basal synaptic transmission is completely normal despite the near elimination of the presynaptic vesicle population, and the loss of synaptic uptake of FM1–43 (Verstreken et al., 2002, 2003; Dickman et al., 2005). This raises the question that STNB may be involved in other processes that affect exocytosis, apart from limiting the availability of vesicles. The observation that viable *stnC* mutants exhibit release defects without major alterations in vesicle pool size (Stimson et al., 1998) seems to support such notion. However, recent findings show that the *stnC* mutation induces the expression of a C-terminally truncated STNB variant, together with low levels of the full-length product (Kelly and Phillips, 2005), thereby possibly involving dominant-negative effects or a partial functionality of the truncated STNB variant. Thus, the physiological phenotype in *stnC* mutants cannot be clearly interpreted. To clarify whether a hypomorphic condition exists that would allow for a segregation of the putative release defect and vesicle pool depletion, we produced a new collection of graded STNB hypomorphic alleles by transgenic expression of STNB in the $stn^{13–120}$ mutant background. In the hypomorphic condition, STNB levels should be sufficient to support vesicle

resupply and to maintain normal vesicle pools, but the shortage would still compromise basal synaptic transmission.

We demonstrate here that physiological defects first emerge when STNB expression is reduced to less than 40% of wildtype level. Below this threshold, the decrease in basal EJC amplitude correlates closely with the expression level of STNB. Hypomorphic *stn-vl* mutants expressing ~35% of the wildtype level are of particular interest for our analysis, because their expression is only slightly lower than this threshold, and yet this condition causes a large 40% drop in basal amplitude. Strikingly, the ultrastructural analysis of *stn-vl* synapses showed that clustered and docked vesicle pools at the presynaptic active zone were completely unaffected in this hypomorphic condition, although there is a slight reduction in overall vesicle density. At the *Drosophila* NMJ, Kuromi and Kidokoro (1998, 2003) previously distinguished an “exo/endo cycling vesicle pool” (ECP) at the bouton periphery, which probably corresponds to the electrophysiologically defined readily releasable pool (RRP; Delgado et al., 2000), and a reserve pool (RP) at the bouton center. According to this study the ECP/RRP alone is sufficient to allow for full-scale basal synaptic transmission after pharmacological depletion of the RP, and a loss of RP vesicles mainly affects synaptic fatigue during HFS. Since our ultrastructural data indicate the integrity of the ECP/RRP in *stn-vl* hypomorphs, it must be concluded that the reduction in average amplitude during low frequency stimulation cannot be simply due to a small vesicle depletion restricted to the RP. Rather, defective basal synaptic transmission must be caused by the reluctant fusion of existing vesicles, correlating with the loss of STNB.

In order to fully characterize this potential adverse effect on exocytosis, we analyzed synaptic response patterns evoked by different stimulation paradigms. Strikingly, *stn-vl* mutants exhibited significantly less pronounced synaptic depression during short stimulus trains applied at different frequencies. Interestingly, altered depression was only found in those low STNB-expressing hypomorphs that also showed defective basal transmission, suggesting a linkage relationship between these phenotypes. A simplistic model of synaptic depression (Zucker and Regehr, 2002) could be satisfied by a progressive depletion of fusion-ready synaptic vesicles during phases of increased activity. Using *shibire* mutants to study depression in the absence of compensating endocytosis, Delgado et al. (2000) previously demonstrated that short trains (5–20Hz) that selectively deplete the RRP caused a depression profile whose shape is reminiscent of the de-staining kinetics of FM1–43 labeled RRP in presynaptic boutons. Hence, the initial phase of depression at NMJ synapses presumably reflects the depletion of the RRP. Based on this interpretation, the altered depression profile in STNB hypomorphs is most likely due to an alteration in mobilization and/or fusion-rate of RRP vesicles. Since abnormal response patterns are also observed for simple paired-pulse stimuli, a shortage of STNB might generally change release properties. It is widely accepted that basal release probability is a determinant factor for short-term plasticity (Thomson, 2000). Indeed, the presence of a depletion-based mechanism of synaptic depression readily implies a dependence of depression kinetics on initial release probability (Zucker and Regehr, 2002). Therefore, the reduction in basal EJC amplitude and the slowing of depression kinetics represent concurring indicators of an underlying decrease of release probability caused by removal of STNB.

Though STNB could in principle play a dual role by independently functioning in exocytosis and endocytosis, we found no evidence to support such hypothesis. In fact, *stn-vl* hypomorphs, which exhibited less pronounced synaptic depression, also demonstrated a delayed recovery after prolonged stimulation indicating an accompanying defect in vesicle recovery. More likely, STNB serves functions on two different levels during vesicle reconstitution: Apart from simply being an essential component constituting functional endocytic complexes, STNB potentially also acts on a governing stage ensuring proper recovery of fusion-competent vesicles. Since a compromised complement of synaptic proteins on recovered vesicles could readily account for the decreased release probability in *stnB* hypomorphs, we assayed for

possible alterations in presynaptic expression levels and localization of synaptic vesicle proteins. While the expression of all tested proteins was at least slightly reduced in *stn-vl* hypomorphs, a definite subset of integral vesicle proteins was clearly most affected by STNB depletion. Synaptobrevin and synapsin expression levels were only slightly (≤30%) reduced, while the abundance of synaptotagmin and vGLUT were more severely decreased (≤50%). Synapsin adheres to available vesicular membranes in a dynamic fashion based on its phosphorylation state (Hosaka et al., 1999) and presumably without obligatory endocytic sorting. Therefore, the reduction in synapsin levels likely represents a decrease in vesicle number within presynaptic terminals. Indeed, this conclusion is well supported by the comparable level of reduction in vesicle density observed at the ultrastructural level. However, the more pronounced effects on synaptotagmin and vGLUT cannot be attributed simply to a physical depletion of vesicles, suggesting a specifically reduced presence in vesicular membranes, consistent with trafficking defects.

A mislocalization of synaptotagmin-1 was already reported by Fergestad et al. (1999) in lethal *stoned* mutants, spawning discussions of a synaptotagmin-focused function of *stoned* proteins. Our new data shows that presynaptic expression of different vesicle proteins was differentially affected by reduced STNB levels, excluding the possibility that defective endocytosis causes an nonselective loss of vesicle proteins from synaptic boutons. Our new data also suggest that STNB function might be important for the correct localization of a specified set of vesicle proteins, which questions whether the loss of synaptotagmin-1 alone is primarily responsible for the physiological phenotypes observed in *stoned* mutants. Based on our finding that *stnB* hypomorphs exhibit impaired neurotransmitter release, and accompanying alterations in vesicle protein configuration, we consider it most likely that STNB acts as a stabilizing and/or sorting factor for several synaptic vesicle proteins supporting this function. Similarly, a recent study by Diril et al. (2006) postulated that the mammalian STNB homolog stonin2 (Martina et al., 2001; Walther at al., 2001) acts as an endocytic sorting adapter for synaptotagmin-1. Confusingly, however, STNB lacks several N-terminal WVxF motifs of its ortholog, which supposedly mediate a stonin2-AP2 interaction crucial for the reported stonin2-induced acceleration of synaptotagmin endocytosis. Nevertheless, association with other AP2-interacting proteins might also enable the recruitment of STNB to appropriate sites.

Synaptotagmin sorting is predicted to critically depend on the ability to interact with the MHD of STNB (Phillips et al., 2000). To examine the role of the MHD-synaptotagmin interaction, we generated targeted mutations to abolish this binding capability. Most interestingly, the complete removal of the MHD, and similarly the introduction of two point mutations within the putative binding interface for synaptotagmin, prevented the expressed STNB protein from restoring viability in lethal *stoned* mutants. Epitope-tagged mutant variant proteins could be neuronally expressed in wildtype animals, but completely failed to localize at synaptic sites. This suggests a crucial role for MHD-based interactions in presynaptic trafficking or anchorage of STNB. It is noteworthy that the STNB Y1125G, R1135A variant could still enter proximal parts of the axon, possibly indicating defective active transport of the protein. In contrast, the C-terminally truncated STNB variant is fully retained in discrete, punctate accumulations within the soma. Surprisingly, a similar, truncated variant of stonin2 seems to distribute uniformly in mammalian neurons (Walther et al., 2004). This might be due to higher expression levels, or different interactions of the remaining N-terminal portion of stonin2. A STNB-AP50 chimera, which contains corresponding sequences of AP50 instead of its original MHD, was also completely missing from synaptic sites, and exhibited punctate somatic localization similar to the truncated STNB variant. Thus, the MHD and the μ2-subunit are not functionally equivalent, even though the transplanted sequences contain the putative synaptotagmin-binding interface (Haucke et al., 2000), and are predicted to confer the ability to bind synaptotagmin. Hence, STNB localization is not dependent on an association with

synaptotagmin. This conclusion is independently confirmed by showing that synaptotagmin null mutants *syt*^{AD4} exhibit only relatively minor changes in STNB localization.

Unlike the well-established SYT-STNB interaction, a direct binding activity between vGLUT and STNB has not been tested to our knowledge. Though the molecular mechanisms of STNB dependent vGLUT localization/stabilization are unclear, several recent studies in mammals (De Gois et al., 2006; Vinatier et al., 2006; Voglmaier et al., 2006) report a direct interaction between its vertebrate homolog, VGLUT1, and endophilin, thereby establishing a connection to the endocytic protein network. It will be very interesting to examine the exact relationship between STNB and vGLUT in the future.

Acknowledgments

We thank Drs. Hugo Bellen, Len Kelly, Erich Buchner, Aaron DiAntonio and Mani Ramaswami for the kind gift of several antibodies and *Drosophila* stocks. We also thank Emma Rushton and Nicole Bibus Christianson for their support and excellent technical assistance. This work was supported by NIH grant GM54544 to K.B.

Abbreviations

AP-2
: adaptor protein complex 2

AP50
: μ2 subunit of AP-2

AZ
: active zone

CME
: clathrin-mediated endocytosis

ECP
: exo/endo cycling vesicle pool

EJC
: excitatory junctional current

EM
: electron microscopy

FM1–43
: *N*-(3-triethylammoniumpropyl)-4-(4-dibutylamino) styryl) pyridium bromide

HEPES
: 4-(2-hydroxyethyl)-1-piperazineethanesulfonic acid

HFS
: high-frequency stimulation

HRP
: horseradish peroxidase

ISI
: interstimulus interval

MHD
: μ2 homology domain

NMJ
neuromuscular junction

OE
over-expressing

PBS
phosphate buffered saline

PAGE
polyacrylamide gel electrophoresis

PCR
polymerase chain reaction

SDS
sodium dodecyl sulfate

PPF/D
paired-pulse facilitation/depression

RP
reserve pool

RRP
readily-releasable pool

S.E.M
standard error of mean

STNA
Stoned A protein

STNB
Stoned B protein

stn-vl/l/m
StonedB hypomorphic mutants with very low/low/moderate expression

SYB
synaptobrevin

SYN
synapsin

SYT
synaptotagmin, TEVC, two-electrode voltage-clamp

UAS
upstream activating sequences

vGLUT
vesicular glutamate transporter

VNC
ventral nerve cord

wt
wildtype

References

Andrews J, Smith M, Merakovsky J, Coulson M, Hannan F, Kelly LE. The stoned locus of Drosophila melanogaster produces a dicistronic transcript and encodes two distinct polypeptides. Genetics 1996;143:1699–1711. [PubMed: 8844157]

Brand AH, Perrimon N. Targeted gene expression as a means of altering cell fates and generating dominant phenotypes. Development 1993;118:401–415. [PubMed: 8223268]

Broadie K, Bellen HJ, DiAntonio A, Littleton JT, Schwarz TL. Absence of synaptotagmin disrupts excitation-secretion coupling during synaptic transmission. Proc Natl Acad Sci U S A 1994;91:10727–10731. [PubMed: 7938019]

Daniels RW, Collins CA, Gelfand MV, Dant J, Brooks ES, Krantz DE, DiAntonio A. Increased expression of the Drosophila vesicular glutamate transporter leads to excess glutamate release and a compensatory decrease in quantal content. J Neurosci 2004;24:10466–10474. [PubMed: 15548661]

De Gois S, Jeanclos E, Morris M, Grewal S, Varoqui H, Erickson JD. Identification of Endophilins 1 and 3 as Selective Binding Partners for VGLUT1 and Their Co-Localization in Neocortical Glutamatergic Synapses: Implications for Vesicular Glutamate Transporter Trafficking and Excitatory Vesicle Formation. Cell Mol Neurobiol 2006;26:679–693. [PubMed: 16710756]

Delgado R, Maureira C, Oliva C, Kidokoro Y, Labarca P. Size of vesicle pools, rates of mobilization, and recycling at neuromuscular synapses of a Drosophila mutant, shibire. Neuron 2000;28:941–953. [PubMed: 11163278]

DiAntonio A, Parfitt KD, Schwarz TL. Synaptic transmission persists in synaptotagmin mutants of Drosophila. Cell 1993;73:1281–1290. [PubMed: 8100740]

Dickman DK, Horne JA, Meinertzhagen IA, Schwarz TL. A slowed classical pathway rather than kiss-and-run mediates endocytosis at synapses lacking synaptojanin and endophilin. Cell 2005;123:521–533. [PubMed: 16269341]

Dickman DK, Lu Z, Meinertzhagen IA, Schwarz TL. Altered synaptic development and active zone spacing in endocytosis mutants. Curr Biol 2006;16:591–598. [PubMed: 16546084]

Diril MK, Wienisch M, Jung N, Klingauf J, Haucke V. Stonin 2 is an AP-2-dependent endocytic sorting adaptor for synaptotagmin internalization and recycling. Dev Cell 2006;10:233–244. [PubMed: 16459302]

Duffy JB. GAL4 system in Drosophila: a fly geneticist's Swiss army knife. Genesis 2002;34:1–15. [PubMed: 12324939]

Estes PS, Jackson TC, Stimson DT, Sanyal S, Kelly LE, Ramaswami M. Functional dissection of a eukaryotic dicistronic gene: transgenic stonedB, but not stonedA, restores normal synaptic properties to Drosophila stoned mutants. Genetics 2003;165:185–196. [PubMed: 14504226]

Fergestad T, Davis WS, Broadie K. The stoned proteins regulate synaptic vesicle recycling in the presynaptic terminal. J Neurosci 1999;19:5847–5860. [PubMed: 10407025]

Fergestad T, Broadie K. Interaction of stoned and synaptotagmin in synaptic vesicle endocytosis. J Neurosci 2001;21:1218–1227. [PubMed: 11160392]

Grigliatti TA, Hall L, Rosenbluth R, Suzuki DT. Temperature-sensitive mutatitions in Drosophila melanogaster. XIV. A selection of immobile adults. Mol Gen Genet 1973;120:107–114. [PubMed: 4631264]

Haucke V, Wenk MR, Chapman ER, Farsad K, De Camilli P. Dual interaction of synaptotagmin with mu2- and alpha-adaptin facilitates clathrin-coated pit nucleation. EMBO 2000;19:6011–6019.

Heuser JE, Reese TS. Evidence for recycling of synaptic vesicle membrane during transmitter release at the frog neuromuscular junction. J Cell Biol 1973;57:315–344. [PubMed: 4348786]

Hosaka M, Hammer RE, Sudhof TC. A phospho-switch controls the dynamic association of synapsins with synaptic vesicles. Neuron 1999;24:377–387. [PubMed: 10571231]

Horton RM. PCR-mediated recombination and mutagenesis. SOEing together tailor-made genes. Mol Biotechnol 1995;3:93–99. [PubMed: 7620981]

Kelly LE, Phillips AM. Molecular and genetic characterization of the interactions between the Drosophila stoned-B protein and DAP-160 (intersectin). Biochem J 2005;388:195–204. [PubMed: 15631619]

Klagges BR, Heimbeck G, Godenschwege TA, Hofbauer A, Pflugfelder GO, Reifegerste R, Reisch D, Schaupp M, Buchner S, Buchner E. Invertebrate synapsins: a single gene codes for several isoforms in Drosophila. J Neurosci 1996;16:3154–3165. [PubMed: 8627354]

Koh TW, Verstreken P, Bellen HJ. Dap160/intersectin acts as a stabilizing scaffold required for synaptic development and vesicle endocytosis. Neuron 2004;43:193–205. [PubMed: 15260956]

Kuromi H, Kidokoro Y. Two distinct pools of synaptic vesicles in single presynaptic boutons in a temperature-sensitive Drosophila mutant, shibire. Neuron 1998;20:917–925. [PubMed: 9620696]

Kuromi H, Kidokoro Y. Two synaptic vesicle pools, vesicle recruitment and replenishment of pools at the Drosophila neuromuscular junction. J Neurocytol 2003;32:551–565. [PubMed: 15034253]

Littleton JT, Bellen HJ, Perin MS. Expression of synaptotagmin in Drosophila reveals transport and localization of synaptic vesicles to the synapse. Development 1993;118:1077–1088. [PubMed: 8269841]

Marie B, Sweeney ST, Poskanzer KE, Roos J, Kelly RB, Davis GW. Dap160/intersectin scaffolds the periactive zone to achieve high-fidelity endocytosis and normal synaptic growth. Neuron 2004;43:207–219. [PubMed: 15260957]

Martina JA, Bonangelino CJ, Aguilar RC, Bonifacino JS. Stonin 2: an adaptor-like protein that interacts with components of the endocytic machinery. J Cell Biol 2001;153:1111–1120. [PubMed: 11381094]

Nicholson-Tomishima K, Ryan TA. Kinetic efficiency of endocytosis at mammalian CNS synapses requires synaptotagmin I. Proc Natl Acad Sci USA 2004;101:16648–16652. [PubMed: 15492212]

Phillips AM, Smith M, Ramaswami M, Kelly LE. The products of the Drosophila stoned locus interact with synaptic vesicles via synaptotagmin. J Neurosci 2000;20:8254–8261. [PubMed: 11069931]

Poskanzer KE, Marek KW, Sweeney ST, Davis GW. Synaptotagmin I is necessary for compensatory synaptic vesicle endocytosis in vivo. Nature 2003;426:559–563. [PubMed: 14634669]

Rohrbough J, Pinto S, Mihalek RM, Tully T, Broadie K. latheo, a Drosophila gene involved in learning, regulates functional synaptic plasticity. Neuron 1999;23:55–70. [PubMed: 10402193]

Rohrbough J, Rushton E, Woodruff E 3rd, Fergestad T, Vigneswaran K, Broadie K. Presynaptic establishment of the synaptic cleft extracellular matrix is required for post-synaptic differentiation. Genes Dev 2007;21:2607–2628. [PubMed: 17901219]

Roos J, Kelly RB. Dap160, a neural-specific Eps15 homology and multiple SH3 domain-containing protein that interacts with Drosophila dynamin. J Biol Chem 1998;273:19108–19119. [PubMed: 9668096]

Schmid SL. Clathrin-coated vesicle formation and protein sorting: an integrated process. Annu Rev Biochem 1997;66:511–48. [PubMed: 9242916]

Sweeney ST, Broadie K, Keane J, Niemann H, O'Kane CJ. Targeted expression of tetanus toxin light chain in Drosophila specifically eliminates synaptic transmission and causes behavioral defects. Neuron 1995;14:341–335. [PubMed: 7857643]

Spradling AC, Rubin GM. Transposition of cloned P elements into Drosophila germ line chromosomes. Science 1982;218:341–347. [PubMed: 6289435]

Stimson DT, Estes PS, Smith M, Kelly LE, Ramaswami M. A product of the Drosophila stoned locus regulates neurotransmitter release. J Neurosci 1998;18:9638–9649. [PubMed: 9822725]

Stimson DT, Estes PS, Rao S, Krishnan KS, Kelly LE, Ramaswami M. Drosophila stoned proteins regulate the rate and fidelity of synaptic vesicle internalization. J Neurosci 2001;21:3034–3044. [PubMed: 11312288]

Thomson AM. Facilitation, augmentation and potentiation at central synapses. Trends Neurosci 2000;23:305–312. [PubMed: 10856940]

Tucker WC, Chapman ER. Role of synaptotagmin in Ca2+-triggered exocytosis. Biochem J 2002;366:1–13. [PubMed: 12047220]

Verstreken P, Kjaerulff O, Lloyd TE, Atkinson R, Zhou Y, Meinertzhagen IA, Bellen HJ. Endophilin mutations block clathrin-mediated endocytosis but not neurotransmitter release. Cell 2002;109:101–112. [PubMed: 11955450]

Verstreken P, Koh TW, Schulze KL, Zhai RG, Hiesinger PR, Zhou Y, Mehta SQ, Cao Y, Roos J, Bellen HJ. Synaptojanin is recruited by endophilin to promote synaptic vesicle uncoating. Neuron 2003;40:733–748. [PubMed: 14622578]

Vinatier J, Herzog E, Plamont MA, Wojcik SM, Schmidt A, Brose N, Daviet L, El Mestikawy S, Giros B. Interaction between the vesicular glutamate transporter type 1 and endophilin A1, a protein essential for endocytosis. J Neurochem 2006;97:1111–1125. [PubMed: 16606361]

Voglmaier SM, Kam K, Yang H, Fortin DL, Hua Z, Nicoll RA, Edwards RH. Distinct endocytic pathways control the rate and extent of synaptic vesicle protein recycling. Neuron 2006;51:71–84. [PubMed: 16815333]

Wall AA, Phillips AM, Kelly LE. Effective translation of the second cistron in two Drosophila dicistronic transcripts is determined by the absence of in-frame AUG codons in the first cistron. J Biol Chem 2005;280:27670–27678. [PubMed: 15951443]

Walther K, Krauss M, Diril MK, Lemke S, Ricotta D, Honing S, Kaiser S, Haucke. Human stoned B interacts with AP-2 and synaptotagmin and facilitates clathrin-coated vesicle uncoating. EMBO Rep 2001;2:634–640. [PubMed: 11454741]

Walther K, Diril MK, Jung N, Haucke V. Functional dissection of the interactions of stonin 2 with the adaptor complex AP-2 and synaptotagmin. Proc Natl Acad Sci U S A 2004;101:964–969. [PubMed: 14726597]

Zucker RS, Regehr WG. Short-term synaptic plasticity. Annu Rev Physiol 2002;64:355–405. [PubMed: 11826273]

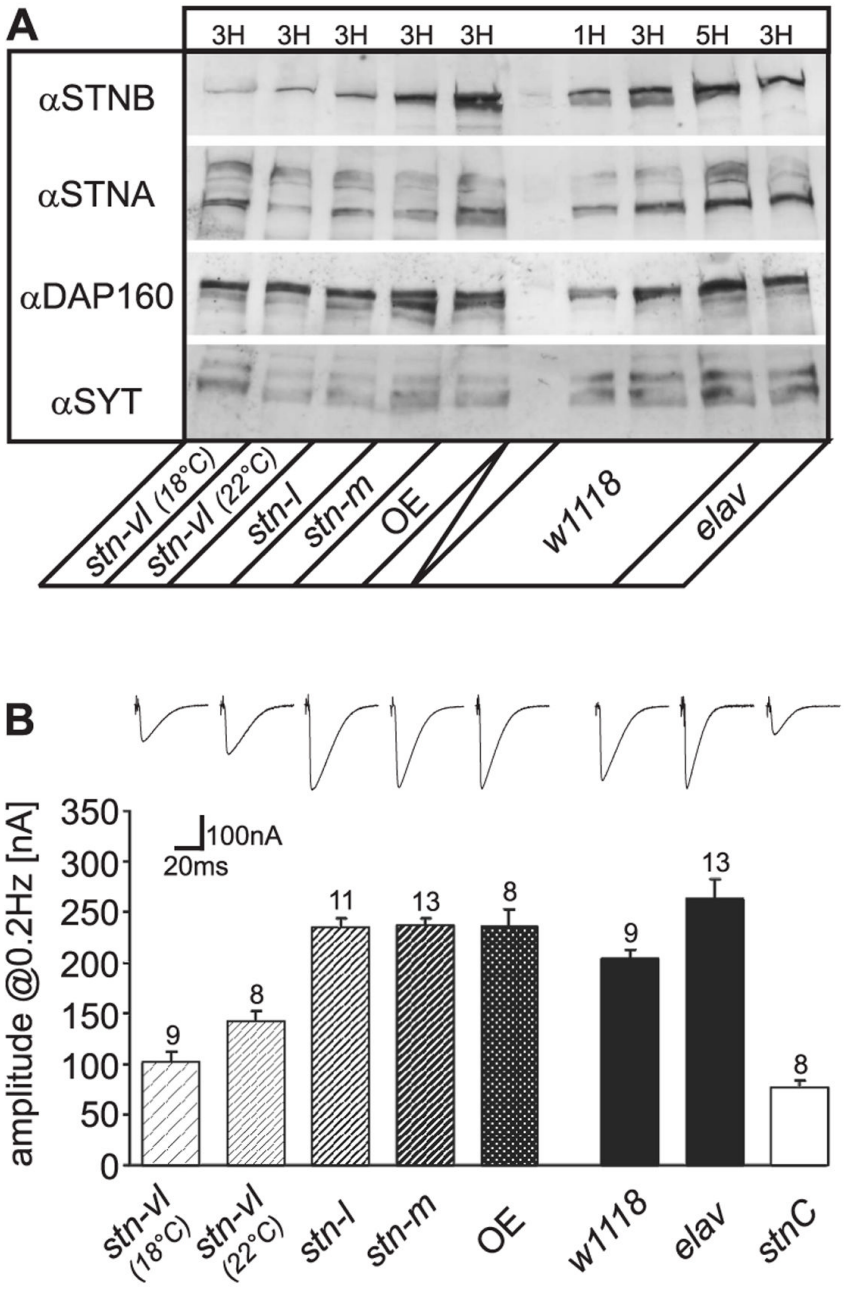

Figure 1. Characterization of novel series of *stnB* hypomorphic alleles

(A) Western blot analysis of *stn-l*, *stn-m* and *stn-vl* (18/22°C) hypomorphs as well as STNB overexpressing (OE) animals; *w1118* and *elav-GAL4* males are controls (right hand section of blot). For each genotype, head extracts were probed with antibodies against STNB, STNA, DAP160 and synaptotagmin (SYT). The amount of protein is indicated in equivalents of extracted fly heads above each lane. STNB expression was manipulated over a wide range using different p{UAS-*stnB*} insertion lines, but little correlated change in the expression levels of putative STNB binding partners or STNA was observed. (B) Characterization of basal synaptic transmission in STNB hypomorphs. Mean EJC amplitudes were assayed in the third instar NMJ (muscle 6, segment A3) at a stimulation frequency of 0.2Hz. In *stn-vl* hypomorphs,

basal synaptic transmission was significantly reduced, and the defect intensified by compromising UAS-GAL4 dependent expression at lower temperature (18°C). Example traces (top panel) represent averages of 10 consecutive EJCs. N is indicated above bars. Error bars depict S.E.M.

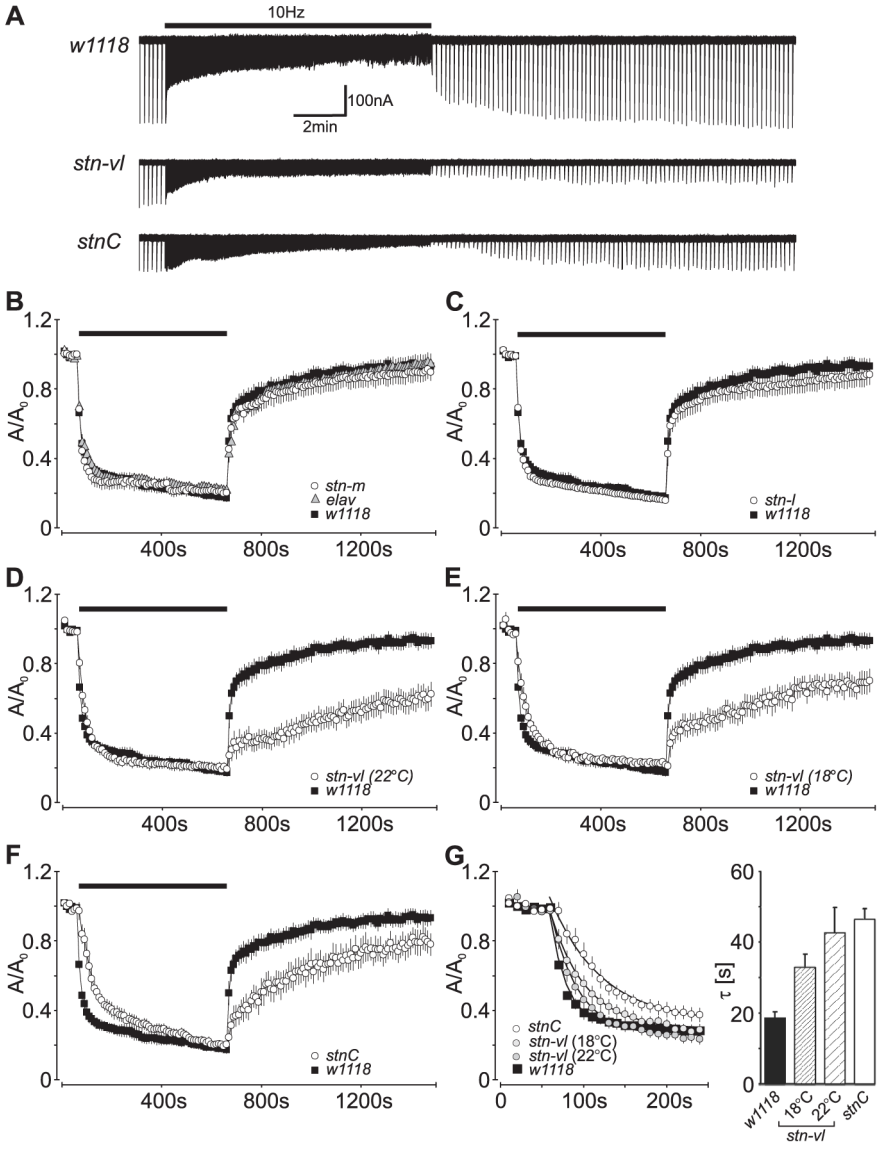

Figure 2. NMJ dynamic properties are altered in *stnB* hypomorphic alleles

(A) Example traces of recordings in larval NMJs of *w1118* controls, *stn-vl* hypomorphs, and *stnC* mutants. EJCs were elicited using a paradigm consisting of a 1min baseline stimulation at 0.1Hz, a 10min interval at 10Hz, and a 14min recovery interval at 0.1Hz. (B-F) Quantification of response profiles in *stn-m* (B; n=7), *stn-l* (C; n=9), *stn-vl* hypomorphs at 22° C (D; n=10) and at 18°C (E; n=11), and *stnC* mutant (F; n=13). *w1118* (black squares in all panels; n=7) and *elav-GAL4* (n=7) serve as controls. The low-expressing *stn-vl* hypomorph exhibited a slowdown in initial depression and an attenuated recovery after stimulation at 10Hz. The depression phenotype was more pronounced if *stn-vl* animals were raised at 18°C, while recovery was slightly facilitated. (G) A plot of the first two minutes during high-frequency stimulation demonstrates the slowdown in depression more clearly (left panel). The monoexponential fit of the data reveals a significant increase in time constants for the depression in *stn-vl* and *stnC* mutants. Error bars represent S.E.M.

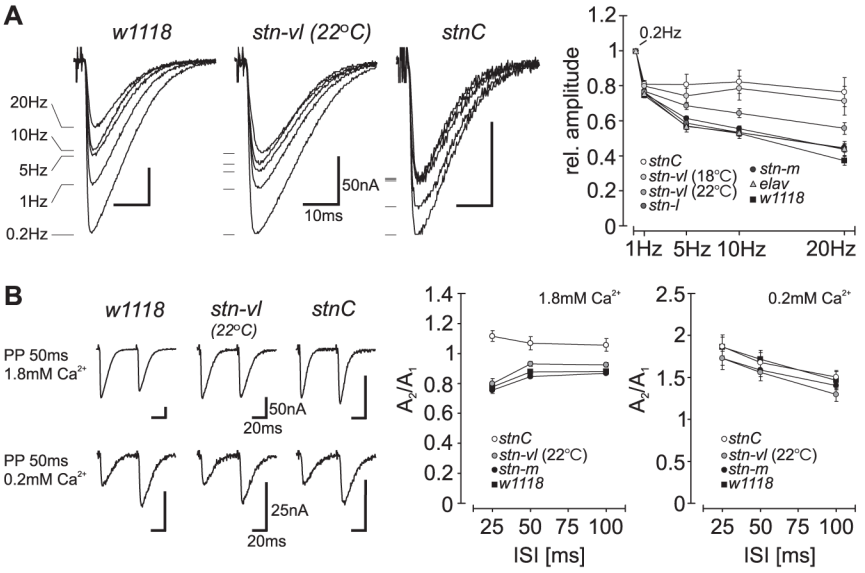

Figure 3. Synaptic depression is reduced in *stnB* hypomorphic alleles

(A) Synaptic depression was assayed by application of short trains of 40 stimuli at different frequencies. The relative amplitude reduction was calculated as the mean amplitude of the last five responses normalized to the baseline amplitude. Representative traces for *w1118* control, and *stn-vl* and *stnC* mutants are depicted in the left hand panel. The quantification (right panel) demonstrates that *stn-vl* (18/22°C) and *stnC* mutants exhibit significantly less relative amplitude depression at stimulation frequencies higher than 1Hz. (B) Synaptic depression during paired-pulse stimulation. Example traces demonstrating paired-pulse depression/facilitation in *w1118*, *stn-vl* and *stnC* are shown in the left panel. Each recording represents an average of 5 consecutive traces. The quantification (right panels) indicates that paired-pulse depression in *stn-vl* (22°C; 1.8mM Ca^{2+}) was slightly but significantly reduced when tested with interstimulus intervals of 50 and 100ms as compared to *w1118* and *stn-m* animals, but was undistinguishable at 25ms. No significant changes could be detected when using low calcium concentrations (0.2mM). N is stated in the text. Error bars represent S.E.M.

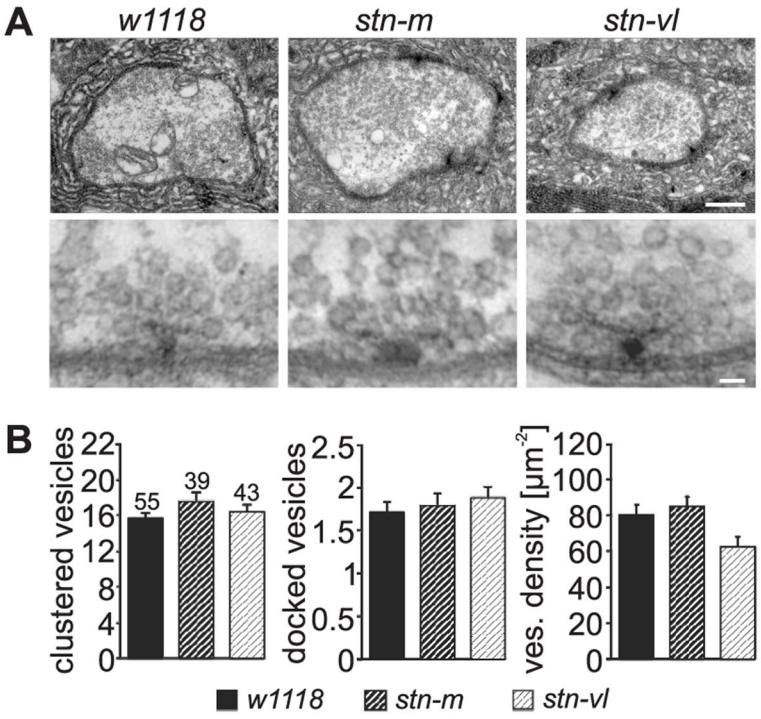

Figure 4. Analysis of NMJ synaptic ultrastructure in *stnB* hypomorphic alleles

(A) Representative third instar NMJ synaptic bouton profiles in *w1118* controls, and moderate *stn-m* and severe *stn-vl* hypomorphs (scale bars: 500nm in upper panel; 50nm in lower panel). (B) Quantitative analysis of ultratructural parameters. The number of clustered (left) and docked vesicles (middle) at presynaptic active zones was similar in all analyzed genotypes. The overall density of vesicles in the bouton was slightly, but significantly reduced in severe *stn-vl* hypomorphs (right). The number of analyzed profiles is indicated above each bar. Error bars represent S.E.M.

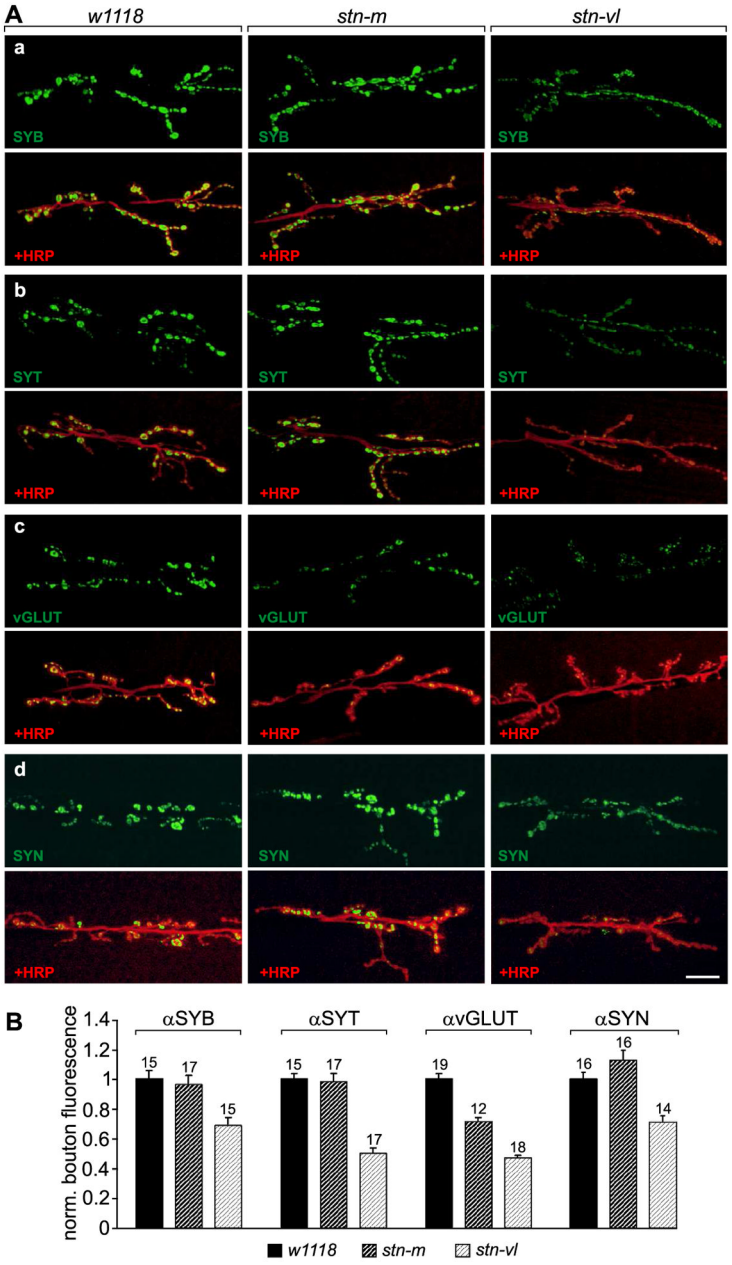

Figure 5. Vesicle proteins are differentially regulated in *stnB* hypomorph alleles

(A) Representative third instar larval NMJs in *w1118* controls (left panel), *stn-m* (middle panel) and *stn-vl* hypomorphs (right panel) labeled for synaptobrevin (SYB) (a), synaptotagmin (SYT) (b), the vesicular glutamate transporter (vGLUT) (c) and synapsin (SYN) (d). The immunofluorescence of each protein is shown alone (in green; upper image) and in superimposition with a marker for the presynaptic membrane (HRP, in red; lower image). The scale bar is 20μm. (B) Quantitative analysis of immunocytochemistry. The expression of SYB and SYN are reduced by ~30% in *stn-vl* (compared to *w1118*), but no reduction was found in the moderate *stn-m* hypomorph. For SYT and vGLUT, a significant stronger reduction of ~50% was observed in *stn-vl*, indicating a differential dependency of synaptic vesicle proteins on STNB. The synaptic expression of vGLUT is also changed in *stn-m* hypomorphs indicating

that the transporter is very sensitive to moderate changes in STNB level. The number of analyzed individual NMJs is indicated above each bar. Error bars represent S.E.M.

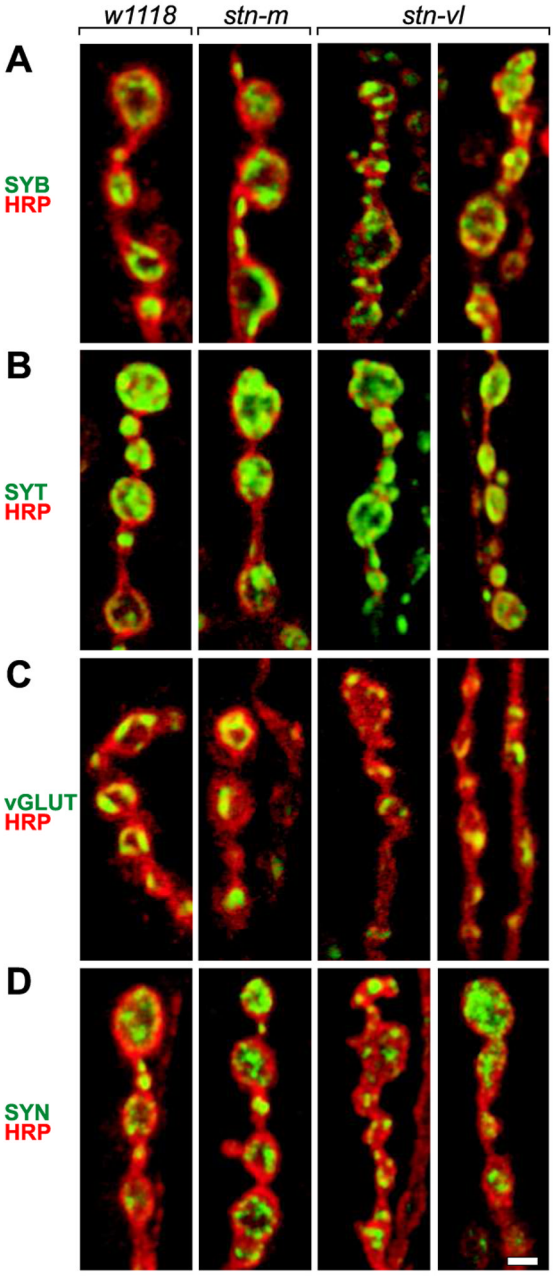

Figure 6. Vesicle protein localization in NMJ boutons of *stnB* hypomorph alleles

High magnification images of third instar NMJ synaptic boutons in *w1118* controls (left column), *stn-m* (middle column), and *stn-vl* (22°C; right columns, terminal and central boutons) probed for synaptobrevin (A; SYB), synaptotagmin (B; SYT), vGLUT (C), and synapsin (D; SYN) (each shown in green). Presynaptic membranes visualized with texas red conjugated anti–horseradish peroxidase antibody (HRP; superimposed in red). NMJs in the severe *stn-vl* hypomorph typically showed deformed presynaptic bouton morphology at terminal boutons of axonal branches, and SYT was systematically mislocalized and shifted towards the presynaptic membrane. The scale bar is 2μm.

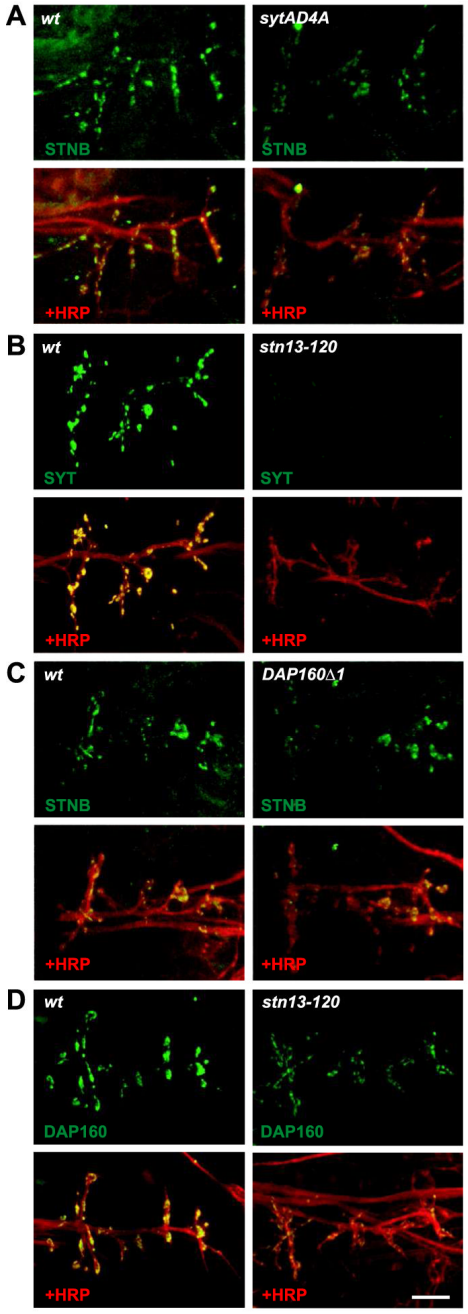

Figure 7. STNB is required to maintain synaptic localization of synaptotagmin

(A) Embryonic NMJs visualized by co-staining with anti-STNB and anti–horseradish peroxidase antibody (HRP; superimposed in lower images). STNB was slightly reduced in syt^{AD4A} null mutants (right) compared to control animals (*wt*; left). (B) SYT in wildtype (*wt*; left), compared to near absence in $stn^{13–120}$ null mutants (right), indicating a strong dependency of SYT on STNB. (C) Synaptic STNB expression is only moderately affected by a loss of DAP160 in $DAP160^{\Delta 1}$ null mutants (right) as compared to control animals (*wt*; left). (D) DAP160 is also moderately reduced in $stn^{13–120}$ null mutants (lower right panel) as compared to control (*wt*; lower left panel). The scale bar is 20μm.

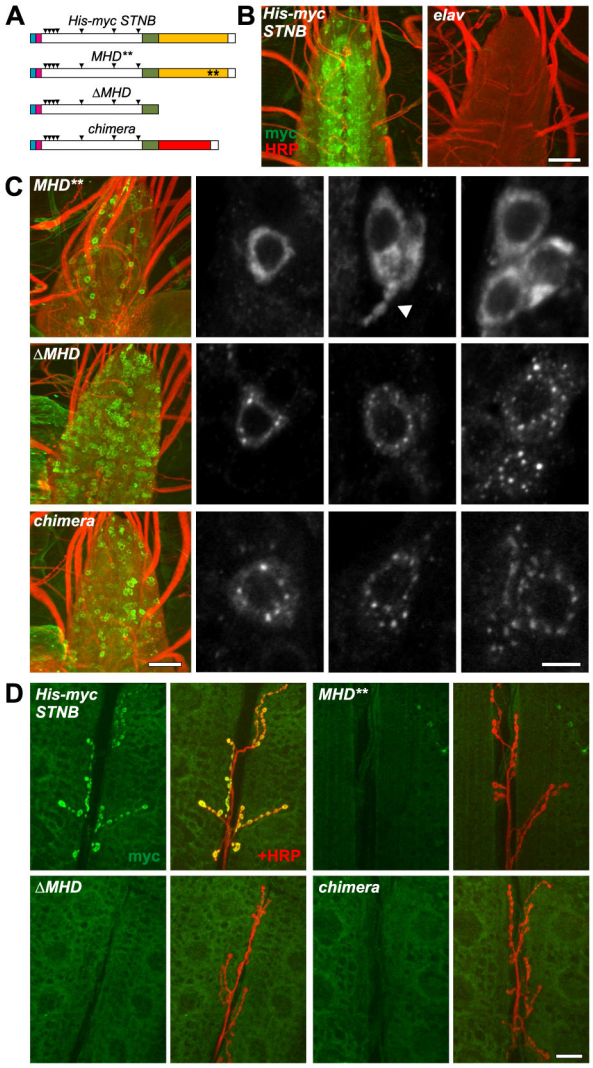

Figure 8. Effects of mutations within the STNB μ2-homology domain (MHD)

(A) The scheme depicts the structure of generated STNB protein variants (blue: His-tag; pink: myc-tag; green: SHD; orange: MHD; red: homologue region of AP50; black triangles: NPF site). Abbreviations are: '*His-myc STNB*' for 6xHis, *myc*-STNB, 'MHD**' for 6xHis, *myc*-STNB Y1125G, R1135A, '*ΔMHD*' for 6xHis, *myc*-STNBΔMHD, and '*chimera*' for 6xHis, *myc-STNB-AP50 chimera.* (B) Pan-neuronally expressed (*elav*-GAL4), myc-tagged STNB correctly localized to the synapse-rich neuropil in the CNS ventral nerve cord (VNC) (green: anti myc, red: anti HRP; left image). The specificity of the immunofluorescent signal was confirmed by staining animals only carrying the *elav*-GAL4 element, but lacking the UAS-construct (right image; scale bar: 20μm). (C) Although the tagged STNB Y1125G, R1135A protein variant was observed in neuronal somata, it was not accumulated in the VNC synaptic neuropil (left picture). Representative images of VNC neuron somata showing a homogenous distribution of STNB (right hand images, 3 examples). Note that STNB Y1125G, R1135A was found in proximal neurite shafts (arrowhead). 6xHis, myc-STNBΔMHD was also observed in VNC neuron soma and was absent from neuropil (left part). High magnification images showing punctate localization in soma (right hand panel, 3 examples). The STNB/AP50 chimera exhibits a very similar localization; absent from neuropil (left image; scale bar: 20μm), and accumulated in soma puncta (right hand images; scale bar: 5μm). (D)

Representative images of third instar larval NMJs (muscles 6/7, segment3) in animals expressing 6xHis, myc-stnB (upper left images), 6xHis, myc-STNB Y1125G, R1135A (upper right images), 6xHis, myc-STNBΔMHD (lower left images) and 6xHis, myc-STNB/AP50 chimera (lower right images). STNB variants without intact MHD were not present in presynaptic boutons, while *myc*-tagged wildtype STNB was normally distributed (left panels: anti myc in green; right panels: merge with anti HRP; scale bar: 20μm).